

More Satellites of Spiral Galaxies

Dennis Zaritsky¹, Rodney Smith², Carlos Frenk³, and Simon D.M. White⁴

¹ Carnegie Observatories, 813 Santa Barbara St., Pasadena, CA, 91101 and UCO/Lick Observatory and Board of Astronomy and Astrophysics, Univ. of California, Santa Cruz, CA, 95064, E-Mail: dennis@ucolick.org

² Department of Physics and Astronomy, P.O. Box 913, University of Wales, College of Cardiff, Cardiff CF2 3YB, Wales, E-Mail: R.Smith@astro.cf.ac.uk

³ Department of Physics, South Road, University of Durham, Durham, DH1 3LE, England, E-Mail: c.s.frenk@durham.ac.uk

⁴ Max-Planck-Institut für Astrophysik, Karl-Schwarzschild-Strasse 1, D-85748 Garching bei München, E-mail: swhite@mpa-garching.mpg.de

Received _____; accepted _____

ABSTRACT

We present a revised and expanded catalog of satellite galaxies of a set of isolated spiral galaxies similar in luminosity to the Milky Way. This sample of 115 satellites, 69 of which were discovered in our multifiber redshift survey, is used to further probe the results obtained from the original sample (Zaritsky *et al.* 1993). The satellites are, by definition, at projected separations $\lesssim 500$ kpc, have absolute recessional velocity differences with respect to the parent spiral of less than 500 km s $^{-1}$ and are at least 2.2 mag fainter than their associated primary galaxy. A key characteristic of this survey is the strict isolation of these systems, which simplifies any dynamical analysis.

We find no evidence for a decrease in the velocity dispersion of the satellite system as a function of radius out to galactocentric radii of 400 kpc, suggesting that the halo extends well beyond 200 kpc. Furthermore, the new sample affirms our previous conclusions (Zaritsky *et al.* 1993) that (1) the velocity difference between a satellite and its primary is not strongly correlated with the rotation speed of the primary, (2) the system of satellites has a slight net rotation (34 ± 14 km s $^{-1}$) in the same sense as the primary's disk, and (3) that the halo mass of an $\sim L^*$ spiral galaxy is in excess of $2 \times 10^{12} M_\odot$.

1. Introduction

Despite the more than 60 years since Zwicky (1933) and Smith’s (1936) measurements of the velocity dispersions in the Coma and Virgo galaxy clusters, and the roughly 20 years since the extended neutral hydrogen galaxy rotation curves of Rogstad and Shostak (e.g. 1971), Bosma (1978) and Rubin, Thonnard, and Ford (1978), we know little about the distribution of the more than 90% of the mass of Universe that consists of dark matter. As we have discussed previously in related work (Zaritsky *et al.* 1993 and Zaritsky and White 1994; hereafter ZSFW and ZW respectively), satellite galaxies are currently the best available probes of the distribution of mass in galaxy halos at large radii (> 100 kpc) from individual galaxies.

In our previous studies, we presented results based on our initial sample of 69 satellites of 45 primaries. In particular, we concluded that the value of the typical halo mass enclosed within a 200 kpc radius lies between 1.5×10^{12} and $2.6 \times 10^{12} M_{\odot}$ (90% confidence limits; ZW). However, those studies left several open questions: (1) does the asymmetric distribution of satellite-primary velocity differences (Arp 1982; Arp & Sulentic 1985; Zaritsky 1992) persist in ever-increasing samples and is it indicative of an interloper fraction much larger than the estimated 0.1 (Zaritsky 1992), (2) will the apparent lack of a correlation between the satellite-primary velocity difference and the primary disk rotation speed persist with increased statistics and a larger range of rotation speeds, (3) is the slight net prograde rotation (29 ± 21 km s $^{-1}$ relative to the primary’s disk rotation; ZSFW) of the satellite system real, and (4) what is the halo mass distribution beyond 200 kpc?

In this paper, we address these questions with our revised and expanded sample of satellite galaxies. We continue to overcome the limitation presented

by the small number of bright satellites around any particular galaxy through a statistical treatment of satellites around a large, well-specified, sample of isolated spiral galaxies. Our fundamental assumption is that an ensemble of satellites belonging to a carefully selected sample of primary galaxies can be treated as if the satellites all belong to a single “typical” primary galaxy. The validity of this assumption depends on the correspondence between the directly observable characteristics of spiral galaxies (such as luminosity) and the indirectly observable characteristics of their dark matter halos (such as mass). The ensemble approach is only viable *either* if there is no correspondence between disk and halo properties or if the correspondence is known. Our previous results suggest that there is little or no correspondence between the mass of the central galaxy and its halo (ZW), thereby supporting our fundamental assumption to even a greater degree than one might naively expect. Nevertheless, one of the principal aims of this study is to further test this assumption.

We present the new satellite sample and discuss some basic observational results. A detailed analysis of the dynamics of the satellite system will be presented elsewhere. We discuss the criteria by which we select primaries and satellites, and the details of how we compile the sample in §2. We address the implications of the new sample on the questions posed above in §3.

2. The Data

2.1. Primary and Satellite Selection

The sample consists of data collected by the authors over the last eight years at a variety of telescopes and from the literature. Satellite identification

and follow-up velocity measurements are described by ZSFW for those satellites included in the first sample. The new satellite identifications are from multifiber redshift surveys at either the Las Campanas Observatories (LCO) or the Anglo-Australian Telescope (AAT).

Once again, we attempt to define a homogeneous sample of isolated primaries. We have slightly modified our criteria from those adopted by ZSFW in order to expand the sample and to test whether some of the previous conclusions depend on the restrictiveness of the selection criteria. Principally, we expand the allowed magnitude range of primaries to examine whether the observed lack of a correlation between the absolute value of the satellite-primary velocity difference, $|\Delta v|$, and the disk rotation speed for the ZSFW sample is due to the smaller range of primary luminosities in that sample. The primaries in the current sample span $-22.4 < M_B < -18.8$ (for $H_0 = 75 \text{ km s}^{-1} \text{ Mpc}^{-1}$ as adopted throughout), although that range is not uniformly sampled (cf. Figure 1). We also relax the criteria against barred primary galaxies. The exclusion of barred galaxies was motivated in ZSFW by the possibility that barred galaxies might reside in halos which are insufficiently massive to suppress bar formation (and so significantly different from the halos of unbarred galaxies). However, the selection of unbarred galaxies is ill-defined because many galaxies are mixed type and close inspection of “unbarred” galaxies can reveal the presence of a small bar (*e.g.*, M51: Zaritsky, Rix, & Rieke 1993). We maintain nearly the same range of allowed recessional velocities as in ZSFW, 1000 to 7500 km s^{-1} . Finally, the isolation criteria remain the same as in ZSFW – all companions within 1000 km s^{-1} in velocity and 500 kpc projected separation must be at least 2.2 mag fainter than the primary and those within 1000 km s^{-1} and between 500 kpc and 1 Mpc projected separation must be at least 0.7 mag fainter.

Our principal source of candidate primaries is the CfA redshift survey catalog (Huchra 1987). A follow-up search for companions and nearby galaxies is done using the NASA Extragalactic Database (NED). Magnitudes for possible nearby bright neighbors are estimated, when not available from NED, using the Space Telescope Digitized Sky Survey in the same manner in which satellite magnitudes are measured (see §2.2 for details). The introduction of quantitative, consistent, and reproducible magnitude measurements is a significant improvement over what was available for ZSFW. This new information has led to the rejection of some fields that were included in ZSFW. In Table 1 we present our justifications for the rejection of certain fields and satellites from the ZSFW sample. In total, 13 satellites from the previous sample are not included in the current sample, principally as a result of the isolation criteria and new magnitude measurements.

Once a sample of suitable primaries is identified, candidate satellite galaxies and their coordinates are obtained either through visual inspection of Palomar or ESO sky survey plates (for the LCO observations) or of APM identified galaxies (for the AAT observations). The selection is susceptible to biases, although it is independent of the most important characteristic of the satellite to us, its recessional velocity relative to the primary. Typically, the satellites are brighter than $m_B = 18.5$ and have angular sizes greater than ten arcsec. No conscious selection (*e.g.*, surface brightness, morphology, or nearness to primary) is introduced. The fiber assignment can introduce some biases (*e.g.*, two candidate satellites separated by a small angular distances cannot both be observed in a single fiber setup), as can the telescope/spectrograph combination (*e.g.*, outer field vignetting decreases the likelihood of observing objects at the edges of the 1.5° diameter field of view). Therefore, as stressed by ZW, a correct dynamical analysis of these data will examine the velocity distribution at each

projected radius, rather than relying on a statistic that incorporates the radial satellite distribution (*e.g.*, the projected mass estimator, $r_p \Delta v^2$).

With the candidate satellites in hand, the next task is to separate satellites from pretenders by measuring recessional velocities. The LCO satellite redshift survey was done with the multifiber spectrograph and 2D-Frutti detector (Shectman *et al.* 1992) on the du Pont 2.5m telescope. The fiber apertures are 3 arcsec in diameter and the fibers are placed manually into a plug plate. A 1200 line mm⁻¹ grating provides wavelength coverage from ~ 3600 to 5300 Å with a resolution of approximately 2.5 Å. The observations occurred during runs in 1992 March, 1993 February, and 1993 November. We typically observed 30 to 40 galaxies per field for two hours in each of 45 fields (combined for the three runs).

The data were reduced using IRAF¹. Velocities are obtained from either the wavelength of bright emission lines or from a cross-correlation analysis (cf. Tonry & Davis 1979). The velocity uncertainty in a single measurement, ~ 70 km s⁻¹, is too large for our dynamical analysis, but is sufficiently precise for the identification of satellites. The fraction of targeted objects for which we measure a redshift is 0.78. Follow-up long-slit observations are obtained to confirm the satellites and measure precise velocities.

Long-slit observations of satellites identified from the multifiber survey and of other satellites that require follow-up observations (*i.e.*, satellites found in the literature with large velocity uncertainties or very faint satellites in ZSFW with dubious velocity measurements) were taken at the 2.5 du Pont telescope

¹IRAF is distributed by the National Optical Astronomy Observatories, which are operated by AURA, Inc., under contract to the NSF.

at LCO using the Modular Spectrograph. A 1200 line mm^{-1} grating provides wavelength coverage from about 4650 to 5900 Å with a resolution of about 3 Å. Although the resolution is comparable to that of the fiber spectra, the stability and linearity of the wavelength solution results in velocities that have 1σ uncertainties of $\leq 20 \text{ km s}^{-1}$ (see below). These long-slit observations were taken in 1993 February, 1993 November, 1994 February, and 1994 November. In addition to observing the satellites, we observed most of the primary galaxies, with the slit placed along the major axis as seen on the acquisition camera, to measure the direction of disk rotation. The observation of primary galaxies also serves as an external test of our velocity measurements (neutral hydrogen measurements are available for most of the primaries from the compilation by Huchtmeier and Richter (1989)).

In Figure 2, we combine primary and satellite velocities for which we have velocities from both the literature and long-slit observations from LCO, and we plot one-half the difference between the two values for each galaxy. The standard deviation from a value of zero is 15 km s^{-1} . We overplot a Gaussian of $\sigma = 15 \text{ km s}^{-1}$ for comparison. Accepted values from the literature typically have quoted uncertainties that are $\lesssim 10 \text{ km s}^{-1}$. Because $|\Delta v|$ is the difference between the primary and satellite velocities, the uncertainty in $|\Delta v|$ is $\sqrt{2} \times \sigma = 21 \text{ km s}^{-1}$. We conservatively adopt a $|\Delta v|$ 1σ uncertainty of 30 km s^{-1} .

The AAT observations were taken during May 1993 using the AUTOFIB automatic fiber positioner feeding the RGO Spectrograph. The 60 fibers each have an angular aperture of 2.1 arcsec. A 1200 line mm^{-1} grating was used with the 25 cm camera and a Tektronix CCD to give a resolution of $\sim 2 \text{ Å}$ and a wavelength range of ~ 4700 to 5500 Å . As many of the fibers as possible were

placed on galaxies such that there was no fixed limiting apparent magnitude. Each field was observed for a total of 8000 sec, split into four 2000 sec exposures.

The AAT data were reduced using the FIGARO spectroscopic data reduction package of the STARLINK suite of astronomical software. Typical velocity errors for spectra with only absorption lines is 20 km s^{-1} , so no follow-up long-slit observations were necessary. Fiber apertures were placed along the major axis of the central galaxy for a few targets, but generally only the redshift of the core of the primary was observed. Unfortunately, the seeing was generally poor, often greater than 3 arcsec, so the success rate at determining redshifts was not as high as for the LCO observations.

The complete sample of satellite galaxies is presented in Table 2. In Column (1) we list the name of the primary (N stands for NGC, I for IC, and A for Anonymous) or the letter designation of the satellite. In Columns (2) and (3) we list the right ascension and declination of the object in 1950.0 epoch coordinates. In Column (4) we present the blue absolute magnitude of the galaxy as given by the apparent magnitude (either from NED, from our own measurements as described below, or from the average of the two when both are available) and the distance as calculated using the primary galaxy's recessional velocity, the simple Virgocentric infall model discussed in ZSFW, and $H_0 = 75 \text{ km s}^{-1} \text{ Mpc}^{-1}$. In Column (5) we list the galaxy's recessional velocity. The recessional velocities for the primaries are from the average of neutral hydrogen observations when available, or from our own observations, and lastly, if neither of those is available (one case, NGC 6948) from the literature at large. The last column (Column 13), which presents the notes, identifies the velocity sources. In Column (6) we list the projected separation in kpc between the satellite and primary. In Column (7) we present our measurement of the galaxy's semimajor

axis length (in kpc). In Column (8) we list the average value of the width of the neutral hydrogen profile at 20% of peak intensity level in km s^{-1} from the compilation of Huchtmeier and Richter (1989). In Column (9) we list the inclination of the galaxy to the line-of-sight. The inclination values come from Huchtmeier and Richter for the primaries and are estimated from the axis ratio as measured from the sky survey plates (see below) for the satellites. In Column (10) we present the angle between the radius vector from the primary to the satellite and the primary’s major axis. In Column (11) we identify whether the satellite has observable emission lines in its spectrum (check means yes, blank means no, ellipses means no spectrum available). In Column (12) we identify whether the satellite is on a prograde or retrograde orbit relative to the rotation of the primary’s disk. Finally, in Column (13) we provide notes on the sources of the recessional velocity data. The code is as follows: H for Huchtmeier and Richter (1989), M for our observations at the MMT telescope (described in ZSFW), N for data from NED, C for our observations at CTIO (described in ZSFW), LC for our long-slit observations at LCO, LCf for our fiber observations at LCO, MX for our observations using the MX Spectrograph at the Steward 2.3m telescope (described in ZSFW), W for our observations using the William Herschel telescope (described in ZSFW), and A for our observations using the AAT.

2.2. Supplementary Data

The sizes and magnitudes of the satellites, and their position angles relative to the primary’s major axis (cf. Table 2) are measured from the Space Telescope Digitized Sky Survey images. Sizes are measured interactively off the monitor

at the faintest surface brightness visible. The magnitudes are measured using the aperture photometry (PHOT) task in IRAF. The aperture is interactively set for each object to the smallest radius at which the magnitude converges. The photometric calibration was done independently for POSS, UK-Schmidt, and 2nd generation POSS survey plates using satellite magnitudes available in the literature. The dispersion about all three calibrations was $\lesssim 0.5$ mag, so we conservatively adopt 0.5 mag as our magnitude uncertainty. Although this approach clearly has pitfalls (*e.g.*, photographic plate non-linear photometry solutions, plate-to-plate variations, poor spatial sampling, and unknown color terms), it is a more quantifiable and robust method than the visual magnitude estimation done by ZSFW. In fact, this new method led to significant revisions in the magnitudes of a few objects, which led to their rejection from the sample (see §2.1 and Table 1).

The magnitude distribution of satellite galaxies is shown in Figure 3. As in ZSFW, the satellites principally have $M_B > -18$ and $3 < \Delta M_B < 5.5$ (Figure 4), suggesting (for the same mass-to-light ratio as their parents) that they are generally between 1/10th and 1/150th as massive as their parents (the mode of the distribution corresponds to a satellite-primary mass ratio of 1:30). As evident in Figure 4, there is no systematic difference in the luminosity distribution of the fiber identified satellites and those identified from the literature.

Average surface brightnesses are estimated using the major and minor axis lengths of the satellites and their magnitudes. The surface brightness can be calculated assuming either that the isophotal ellipticities reflect true asymmetries in the galaxy (and so no inclination correction is included) or that the ellipticities are directly due to inclination and that the galaxy is optically

thin. We show the relationship between surface brightness and projected separation in Figure 5 for both treatments. The correlation between surface brightness and projected separations is statistically insignificant in both panels.

Our determination of whether an object has emission lines is based on a visual examination of the observed spectra. We possibly miss emission lines due to the placement of the fiber or slit on the object, or due to the low signal-to-noise of the lines; however, there is no bias that will produce spurious emission lines. Of the satellites for which we obtained spectra, 86% have detectable emission lines.

The orbital orientation of a satellite is determined for the 57 systems for which the direction of the primary’s spin has been measured. The satellite is on a prograde, “p” orbit if its recessional velocity is in the same sense as the side of the disk nearest to it, and retrograde, “r”, otherwise.

3. Discussion

3.1. “Numerology”

The new sample of satellites consists of 115 satellites around 69 primaries. These are divided almost equally between satellites presented in ZSFW and new satellites (56 vs. 59, respectively), and there are about 1.5 times as many fiber satellites as literature satellites (69 vs. 46, respectively; where satellites “rediscovered” in the multifiber surveys are categorized as fiber satellites).

As shown in Figure 6, systems range from very rich (with 4 or 5 members), which are suspiciously like galaxy groups, to single satellite members. The groups are a particularly important class because they have the potential to

skew statistics in a correlated manner. For example, if the five satellites of NGC 1961 are in fact a group projected near NGC 1961, then they could conceivably *all* have large projected separations and velocity differences. Physically, there may also be subtle dynamical interactions between the satellites themselves, which are missed when satellites are treated as independent particles. The average number of satellites per primary, for primaries with detected satellites, is 1.7. This average is slightly larger than the 1.5 average for the ZSFW sample. In both cases, this average represents a lower limit to the number of satellites because the surveys are incomplete.

The decline in the number of systems with satellite richness (Figure 6) is quite regular. If we treat the presence of a satellite as a random event with probability, p , then the probability of finding a system with n satellites is p^n . We fit this expression to the numbers of systems with $n = 1, 5$ to find the effective number of fields observed and p . The best fit value for the probability of finding a satellite around an isolated spiral galaxy and within the magnitude range we probe is 0.43 ± 0.06 and the fit to the data has $\chi^2 = 0.38$. We also find that the effective number of fields searched is 94 ± 25 , which implies that the average number of satellites per field spiral galaxies is 1.2 ± 0.3 . We overplot this model in Figure 6. The quality of the fit supports the assumption that the satellites are independent (*e.g.*, they do not preferentially come in pairs), which simplifies any analysis and justifies treating each satellite as an independent datum, and that the typical galaxy has at least one satellite, which implies that spiral galaxies with satellites are not an atypical subset of spirals.

3.2. The Asymmetry of the Satellite Velocity Distribution

The distribution of satellite galaxy velocities, and to a lesser extent binary galaxy velocities, are skewed so that a satellite, or the fainter of two binary galaxies, has a greater than 50% probability of having a larger recessional velocity than the primary galaxy (Arp 1982; Arp & Sulentic 1985; Zaritsky 1992). The naive expectation, when dealing with a system of presumably bound objects, is that satellite recessional velocities will be divided equally into approaching and receding objects. The asymmetry (present in existing samples at a level of about 59:41, receding to approaching satellites for the projected separation criteria of this study; Zaritsky 1992) has been interpreted by some (Arp 1982; Arp & Sulentic 1985) as an indication of a non-Doppler component of the redshift. Zaritsky (1992) presented an analysis of the existing satellite samples and concluded that observational biases in the selection of satellite galaxies naturally leads to a slight velocity asymmetry and that the observed asymmetry was consistent with those biases plus counting statistic fluctuations in the ZSFW sample. However, if the asymmetry persists at the same level in ever increasing samples, the effect would become more and more difficult to explain in terms of selection biases and counting statistics.

The current sample still has an excess of positive Δv satellites, although at a lower level than the ZSFW sample. If we quantify the asymmetry by the ratio of the number of satellites with positive Δv to the total number of satellites, P/T , then the current sample has $P/T = 0.57$, relative to $P/T = 0.59$ for the ZSFW sample. Treating the satellites as purely independent trials and assuming equal probabilities for negative and positive Δv , the probability of this asymmetry in a sample of 115 satellites is 0.07. ZSFW noted that most of the asymmetry in their sample appears to come from the literature sample rather than the fiber sample. Dividing our sample into literature and fiber samples illustrates that

that impression is borne out by the current sample. The literature sample has $P/T = 0.61$, while the fiber sample has $P/T = 0.54$. The former has only a probability of 0.09 of occurring, while the latter has a probability of 0.28. The fiber sample is therefore entirely consistent with a random distribution (and even more consistent with the expected distribution, which should be slightly asymmetric due to observation selection effects (Zaritsky 1992)).

Because unknown physical phenomena, which might cause the observed effect, would affect the literature and fiber samples equally, we assert that selection biases are the dominant cause of the asymmetric Δv distribution. The literature sample must be skewed because it contains more correlated systems (i.e. projected groups), for which binomial statistics underestimate the probability of the observed asymmetries. We conclude, because the level of asymmetry has declined slightly as the sample has grown and because the fiber sample appears to be free of significant contamination, that the total sample is consistent with the previous estimate of the interloper fraction in this type of sample (~ 0.1). As we discuss next, other properties of the satellite ensemble further support our conclusion that interlopers are not a dominant fraction of the sample.

3.3. The Disk-Halo Connection?

ZSFW noted that $|\Delta v|$ and the primary’s disk rotation velocity appear to be uncorrelated (in fact there is a slight anti-correlation in the ZSFW sample). An analogous lack of correlation was also seen in samples of binary galaxies (White *et al.* 1983; Charlton & Salpeter 1991). The infall model of ZW allowed for the possibility that halo and disk masses may not track each other, but no physical

motivation for that behavior was presented. Since then, numerical simulations of the process of galaxy formation have suggested that a strong correlation should not be expected between the two quantities (Navarro, Frenk, & White 1996).

In Figure 7 we plot $|\Delta v|$ vs. $1/2$ the inclination corrected value of the H I profile width for the associated primary (the amplitude of the rotation curve), $0.5W_i$. There is no apparent correlation between the two quantities, regardless of whether the objects with $|\Delta v| > 250$ km s $^{-1}$ are treated as interlopers or not. At a low significance level, there may be an indication that galaxies with $0.5W_i < 200$ km s $^{-1}$ have satellites with smaller than average $|\Delta v|$'s. Given the recent results from simulations on the behavior of disks and halos, the lack of a strong signal is not as surprising as it once was and may be consistent with the parameterization of halo rotation curves found by Navarro *et al.* (1996).

The second aspect of the disk-halo connection that we examine is the net prograde rotation of the satellite system found by ZSFW. Their measurement of the net rotation was just slightly more than 1σ different from zero net rotation (29 ± 21 km s $^{-1}$). The new value of the net rotation velocity, 34 ± 14 km s $^{-1}$, confirms and strengthens the previous observation of a slight net prograde rotation of the satellite systems.

The histogram of velocities is shown in Figure 8. As in the smaller ZSFW sample, the peak in the distribution appears at small retrograde velocities and the distribution has an asymmetric tail to large prograde values. This asymmetry is an entirely different one from that in Δv . Because any interlopers should be evenly distributed between prograde and retrograde velocities, this asymmetry suggests that at least some objects with large $|\Delta v|$, which are typically assumed to be interlopers, may be associated with their respective primary galaxy.

Lastly, the azimuthal distribution of satellites with respect to the disk plane is elongated perpendicular to the disk plane at radii > 300 (Zaritsky *et al.* 1996) and suggests that interlopers are not the dominant population at large radii. Therefore, both the spatial distribution and the connection between velocities and disk spin suggest that some of the systems that one might suspect to be interlopers are physically associated with the primary galaxy.

3.4. Radial Velocity vs. Projected Separation

As suggested in §3.2 and 3.3, the sample is not strongly contaminated by interlopers and so should provide a reliable probe of outer halo dynamics. In Figure 9 we plot the distribution of Δv vs. projected separation, r_p . The large majority (100 of 115) of satellites have Δv ’s between ± 200 km s $^{-1}$ indicating that the “satellites” are indeed associated with (but not necessary gravitationally bound to) the primary. The general behavior of the distribution is identical to that of the ZSFW sample. The most noticeable change is the increased sampling of the distribution at radii ~ 400 kpc.

The influence of the dark matter halo on the satellite velocities is evident in Figure 10, where we have plotted $|\Delta v|$ vs. r_p . There is no apparent decline in the velocity dispersion of satellites as a function of radius. Visual comparison with the models shown in Figure 2 of White and Zaritsky (1992) suggests that halos with mass profiles characteristic of $\Omega_0 < 0.3$ models will be strongly ruled out. The median $|\Delta v|$ of satellites at projected separations > 243 kpc, a radial range chosen for direct comparison to ZSFW, is 78 km s $^{-1}$, slightly larger than the value of 67 km s $^{-1}$ obtained for the ZSFW sample. This agreement suggests that the ZSFW and ZW results regarding the mass of halos are unlikely to

change dramatically once this new sample is carefully analyzed.

4. Conclusions

We have constructed a revised and enlarged sample of satellite galaxies around isolated spiral galaxies. With this sample we have addressed several questions regarding the nature of galaxy halos. In particular, we find that

- (1) the probability of finding a satellite around these isolates spiral primaries, for systems having from 1 to 5 satellites, is described by $P = 0.4^n$, where n is the number of satellites (the probability of not finding a satellite in a system is then 25%),
- (2) the new sample has a less asymmetric Δv distribution than the ZSFW sample, and more importantly, the satellites identified from our fiber survey, for which the selection criteria and biases are best known, show no significant Δv asymmetry,
- (3) the primary's disk rotation speed and $|\Delta v|$ still show no significant correlation,
- (4) the net prograde rotation of the satellite system with respect to the primary disks is confirmed and is now measured to be $34 \pm 14 \text{ km s}^{-1}$, and
- (5) the lack of any clear dependence between the velocity dispersion of the satellite system and projected radius is even more striking than in the ZSFW sample, thereby supporting the previous conclusion of large and massive galaxy halos.

The revised and expanded satellite sample presented here has illuminated three key reasons for believing that most of the identified satellite galaxies are indeed related to their primaries (1) the high concentration of galaxies at $|\Delta v|$

< 200 km s $^{-1}$ (87% of the sample), (2) the net prograde rotation of the system relative to the disk rotation (distinct from zero rotation at the 98.5% confidence level), and (3) the asymmetric azimuthal distribution of satellites, with the major axis of the distribution at large radii aligned with the minor axis of the disk (Zaritsky *et al.* 1996). This new sample confirms the result of large and massive dark matter halos around isolated spiral galaxies (ZSFW and ZW), but it also begins to provide detailed information about the distribution and orbits of outer halo material. Because of the long dynamical timescale at large radius, the behavior of this material may provide our best probe of the initial characteristics of galaxy halos.

Acknowledgments: DZ acknowledges partial financial support from the California Space Institute and from NASA through HF-1027.01-91A, from STScI, which is operated by AURA, Inc., under NASA contract NAS5-26555.

References

Arp, H. 1982, ApJ, 256, 54

Arp, H., & Sulentic, J.W. 1985, ApJ, 291, 88

Bosma, A. 1978, Ph.D. Dissertation, Univ. of Groningen

Charlton, J.C., & Salpeter, E.E. 1991, ApJ, 375, 517

Huchra, J. P. 1987, *The CfA Redshift Catalogue*

Huchtmeier, W. K., and Richter, O.-G. 1989, *H I Observations of Galaxies*, (New York: Springer-Verlag) (HR)

Ingerson, T. E. 1987, in *Instrumentation for Ground-Based Optical Astronomy*, ed. L.B. Robinson (New York: Springer-Verlag), p. 222

Ingerson, T. E. 1988 in *A.S.P Conference Series Vol. 3, Fiber Optics in Astronomy*, ed. S.C. Barden (Provo: Astronomical Society of the Pacific), p. 99

Lorrimer, S. J., Frenk, C. S., Smith, R. M., White, S. D. M., and Zaritsky, D. 1994, MNRAS, 269, 696

Navarro, J.F., Frenk, C.S., & White, S.D.M 1996, preprint

Rogstad, D.H., & Shostak, G.S. 1971, AA, 13, 99

Rubin, V.C., Ford., W. K., Jr., and Thonnard, N. 1978, ApJL, 225, L107

Schmidt, G., Weymann, R. J., and Foltz, C. B. 1989, PASP, 101, 713

Shectman, S.A., Schechter, P.L., Oemler, A.A., Tucker, D., Kirshner, R.P., & Lin, H. 1992, in *Clusters and Superclusters of Galaxies* (ed. Fabian, A.C.), (Kluwer: Dordrecht), p. 351

Smith, S. 1936, ApJ, 83, 23

Tonry, J., and Davis, M. 1979, AJ, 84, 1511

White, S.D.M. 1981, MNRAS, 195, 1037

White, S.D.M., Huchra, J., Latham, D., & Davis, M. 1983, MNRAS, 203, 701

White, S.D.M., & Zaritsky, D. 1992, ApJ, 394, 1

Zaritsky, D., 1992, ApJ, 400, 74

Zaritsky, D., Rix, H.-W., & Rieke, M. 1993, Nature, 364, 313

Zaritsky, D., Smith, R., Frenk, C. S., & White, S. D. M., 1993, ApJ, 405, 464

Zaritsky, D., & White, S.D.M. 1994, ApJ, 435, 599

Zwicky, F. 1993, *Helv. Phys. Acta*, 6, 110

Table 1: Cause for Omission of ZSFW Data

N259a	At high redshift (45,400 km s ⁻¹) from follow-up spectroscopy
N1459 Field	Galaxy at $r_p = 792$ kpc with $\Delta m_B = 0.2$
N4679 Field	Galaxy at $r_p = 120$ kpc with $\Delta m_B = 1.3$
N5073 Field	N5073b has $\Delta m_B = 1.5$
N5085 Field	N5085a superposed on a bright star (current Δm_B estimate is 1 mag)
N5254 Field	N5254a has $\Delta m_B = 1.5$
N5297 Field	N5297a has $\Delta m_B = 1.5$
N5768 Field	N5768a has $\Delta m_B = 1.1$
N6943b	CTIO velocity was not confirmed with follow-up spectroscopy (no reliable velocity measured)
A2120 Field	Galaxy at $r_p = 435$ kpc with $\Delta m_B = 1.7$
N7083 Field	Galaxy at $r_p = 409$ kpc with $\Delta m_B = 1.0$
N7716 Field	N7716a has $\Delta m_B = 1.5$

Figure Captions

- 1 – The distribution of blue absolute magnitudes, M_B , for the primary galaxies.
- 2 – Velocity measurement reproducibility. We plot the difference between Las Campanas long-slit measurements and the average of long-slit and literature values for both primary and satellite galaxies observed at Las Campanas. We overlay a Gaussian with $\sigma = 15 \text{ km s}^{-1}$ and mean = 0 for comparison (the Gaussian is not a fit to the data).
- 3 – The distribution of blue absolute magnitudes for the satellite galaxies. The unshaded histogram represents the entire sample, while the shaded one represents only those satellites discovered from the fiber surveys. The location of Local Group galaxies are added at the top for comparison.
- 4 – The distribution of primary-satellite magnitude differences. The unshaded histogram represents the entire sample, while the shaded one represents only those satellites discovered with the fiber surveys.
- 5 – The distribution of satellite average surface brightness versus projected separation. The top panel contains average surface brightnesses over the projected area of the satellite (πab , where a and b are the satellites semimajor and semiminor axis). The bottom panel contains average surface brightnesses over the deprojected area (πa^2).
- 6 – The distribution of the systems as a function of satellite number. The connected dots represent the best fit model assuming that the presence of a satellite is a random variable (probability of finding n satellites around a field spiral galaxy is proportional to 0.43^n).
- 7 – $|\Delta v|$ vs 0.5 times the inclination corrected neutral hydrogen profile width, $0.5W_i$.

8 – Distribution of satellite radial velocities relative to the disk. Positive velocities represent prograde satellites, while negative ones represent retrograde satellites.

9 – The distribution of Δv vs r_p for the satellite galaxies. Filled circles represent satellites from the fiber surveys and crosses represent those found from literature surveys.

10 – The distribution of $|\Delta v|$ vs. r_p for the satellite galaxies.

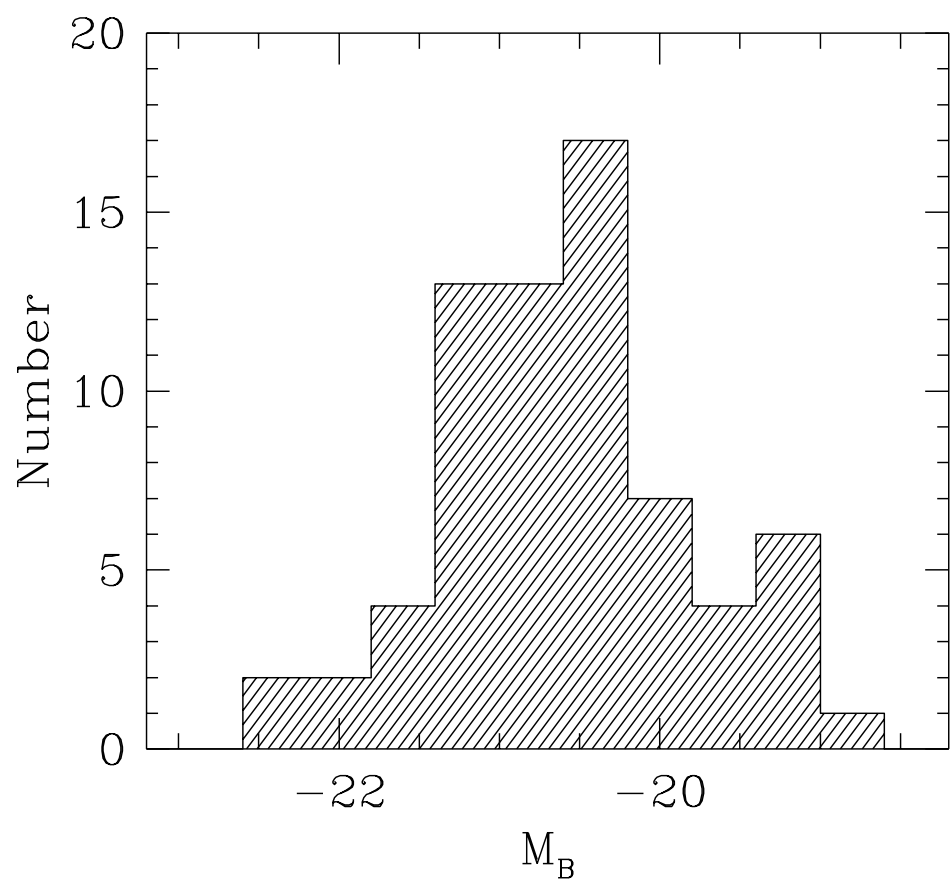


Fig. 1.—

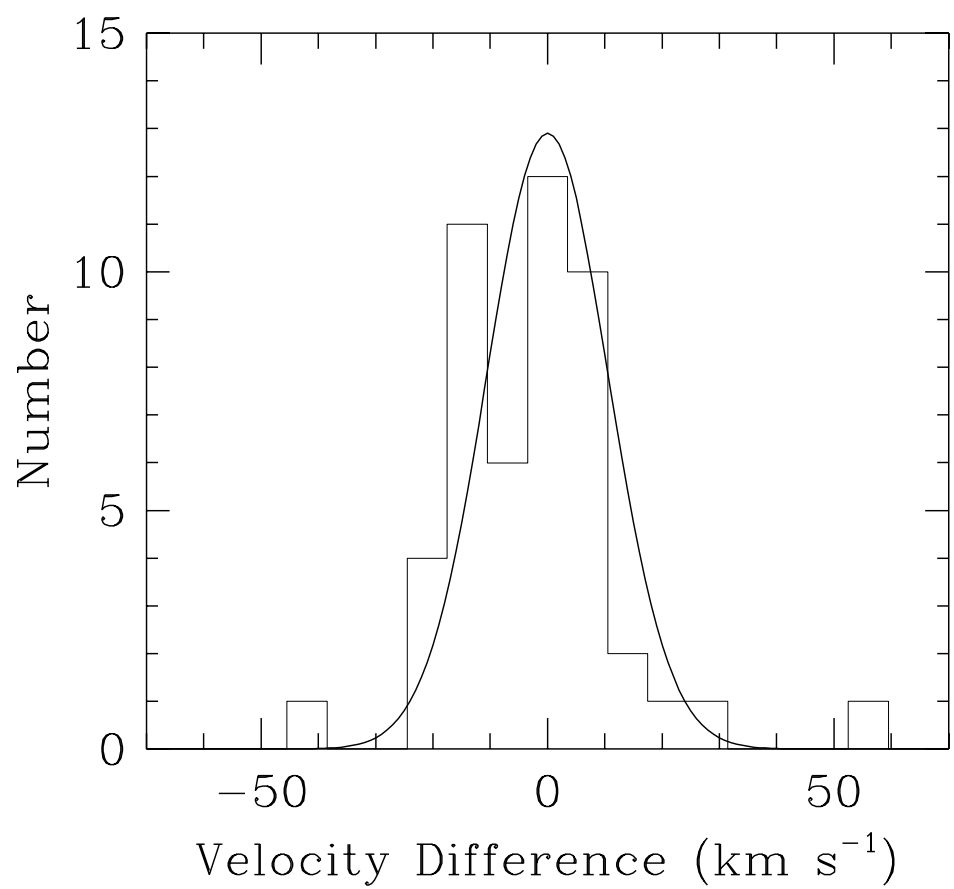


Fig. 2.—

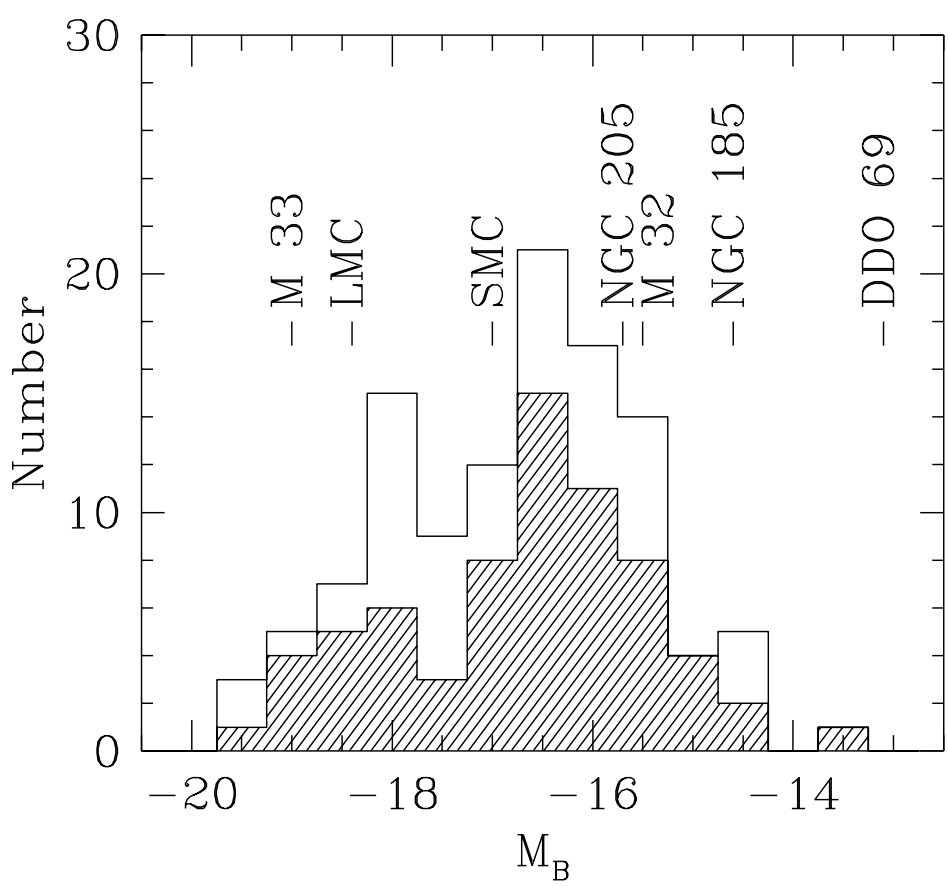


Fig. 3.—

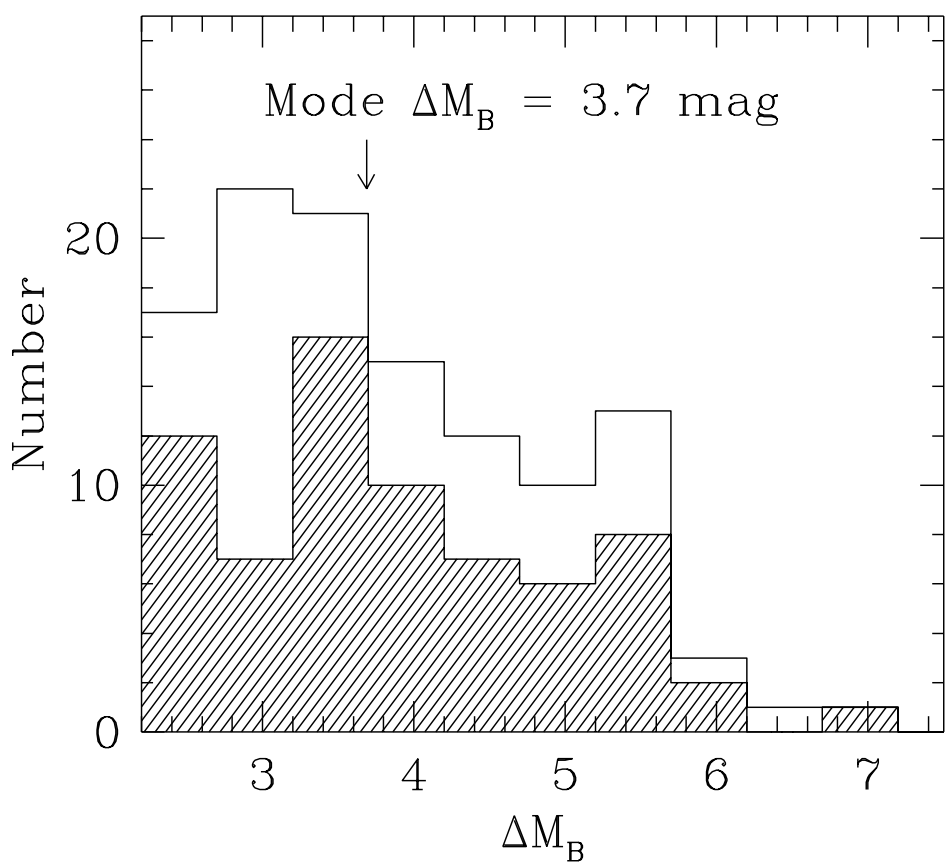


Fig. 4.—

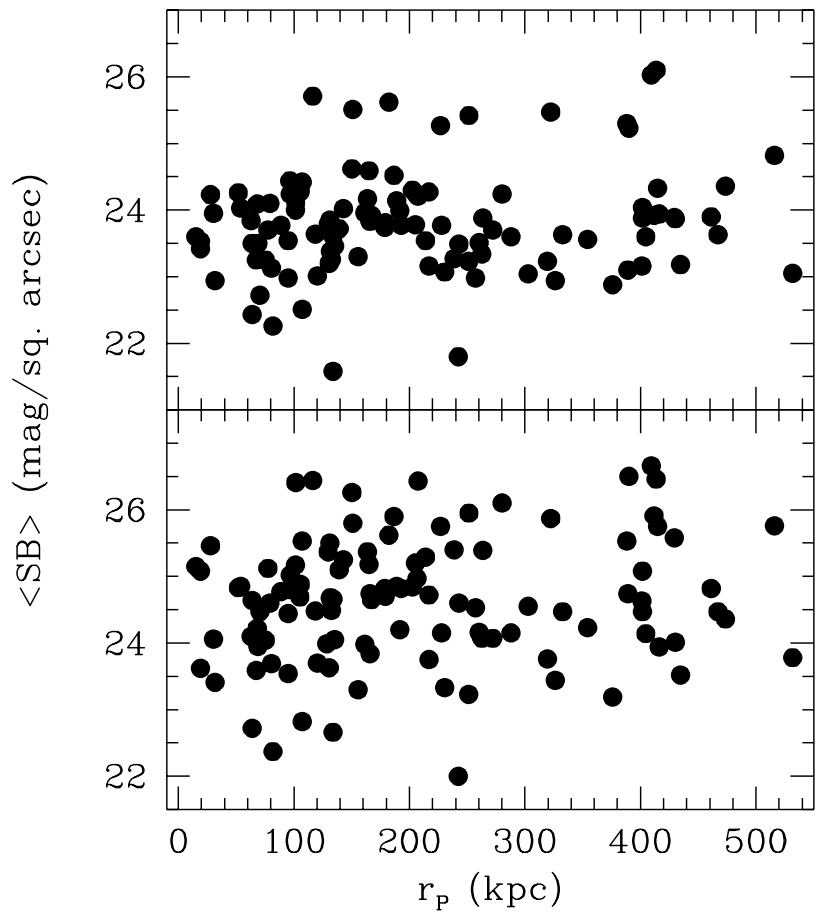


Fig. 5.—

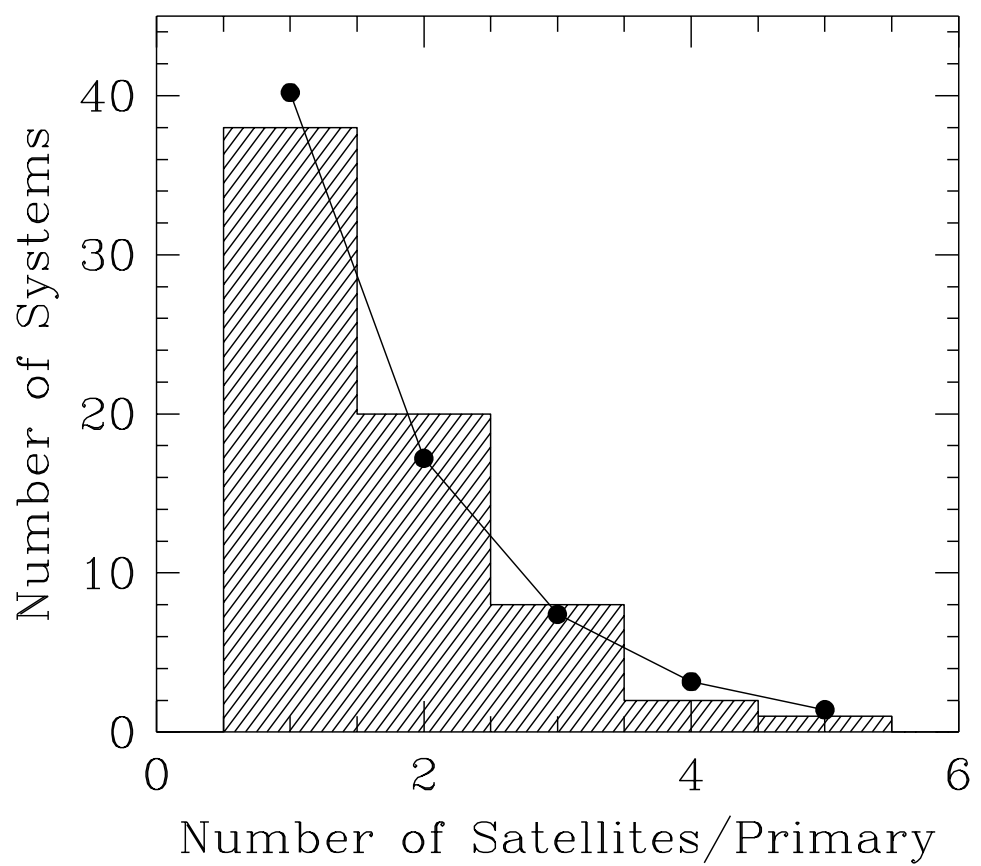


Fig. 6.—

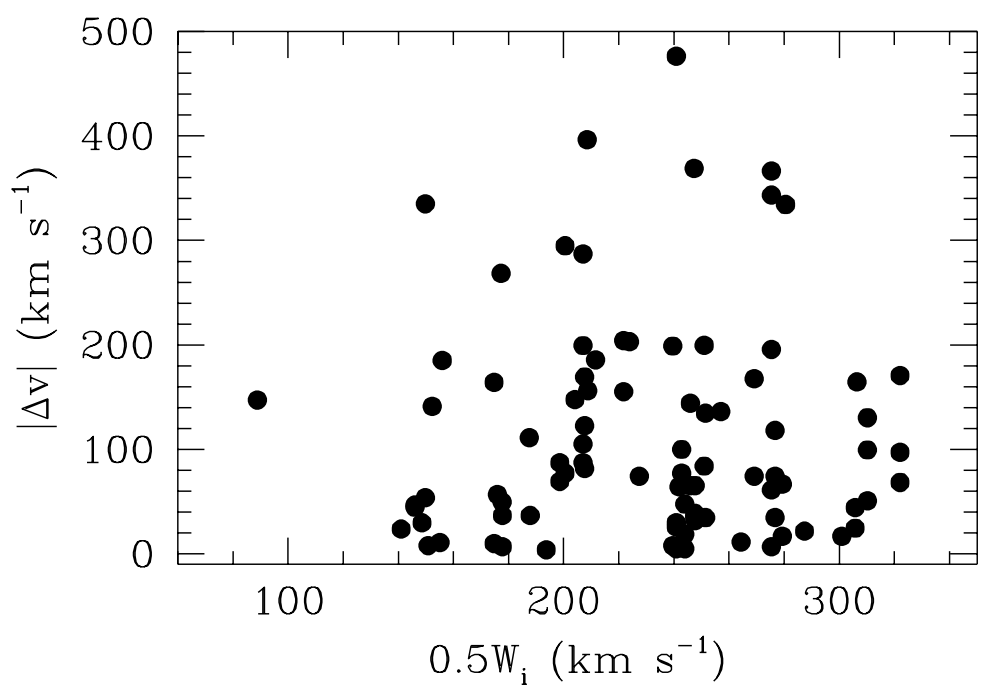


Fig. 7.—

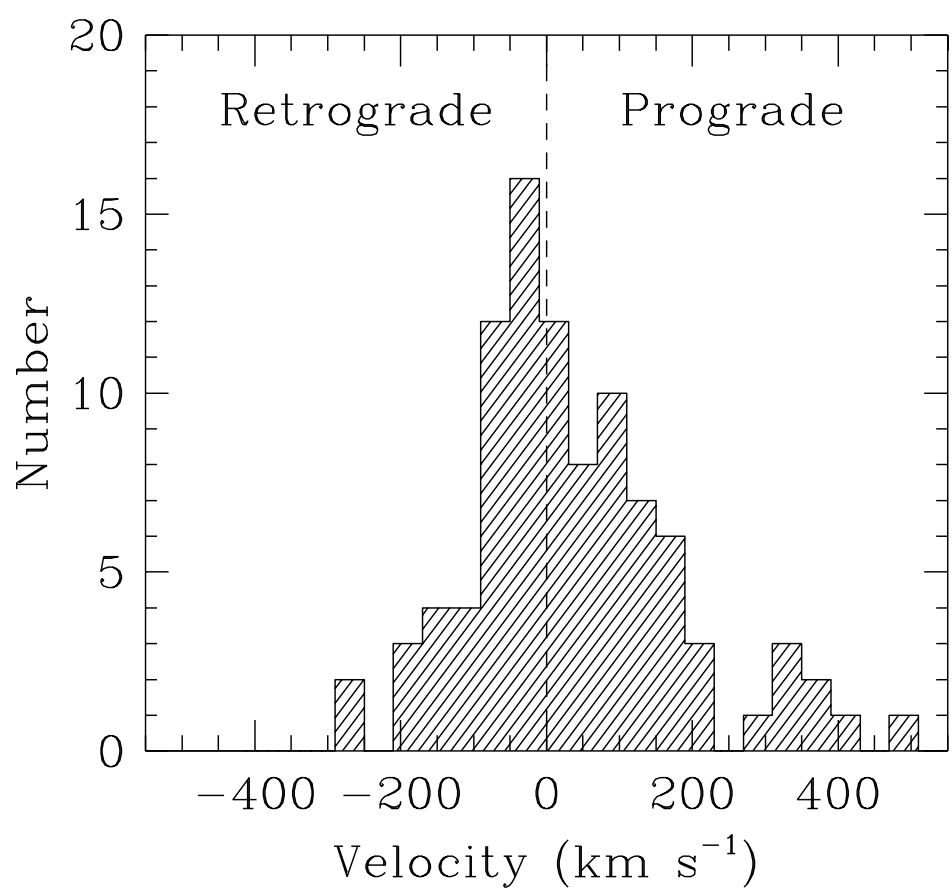


Fig. 8.—

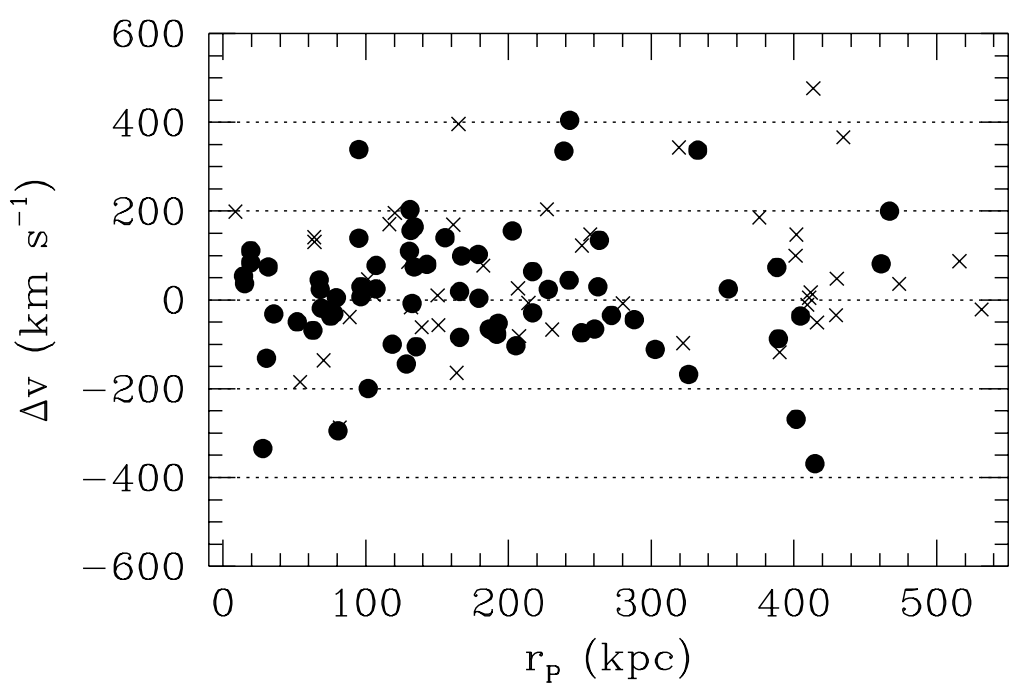


Fig. 9.—

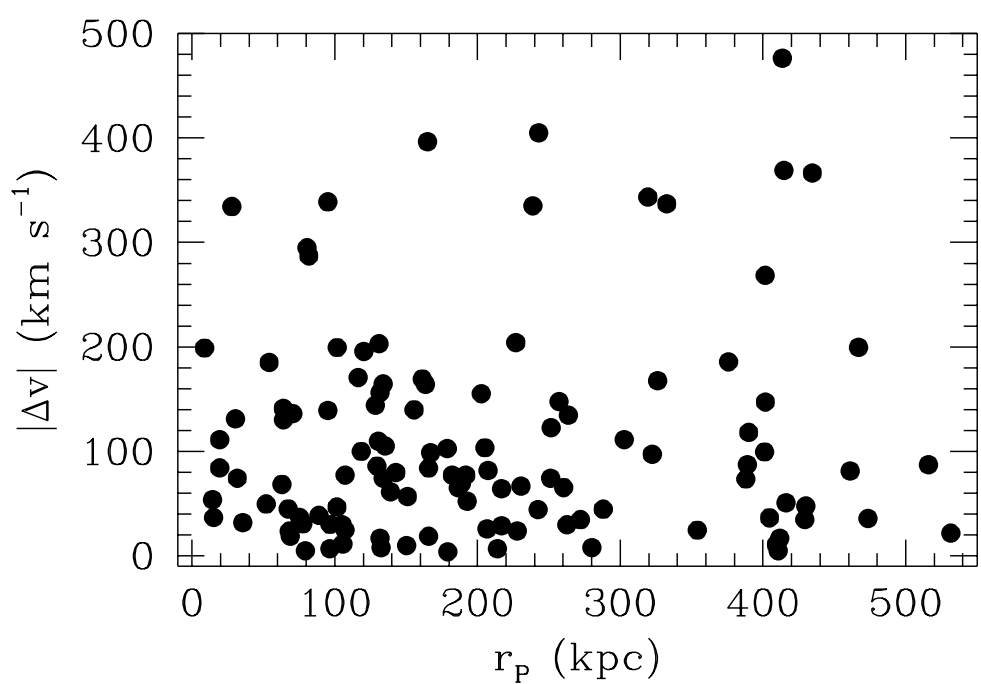


Fig. 10.—